Quantum Dynamics Study of the Excited-State Double-Proton Transfer in 2,2′-Bipyridyl-3,3′-diol

Ricard Gelabert, Miquel Moreno, and José M. Lluch*[a]

Density functional theory and quantum dynamics simulations have been used to study the double-proton transfer reaction in 2,2′-bipyridyl-3,3′-diol in the first singlet excited electronic state. This process is experimentally known to be branched: It consists of a fast, concerted reaction mechanism ($\tau \approx 100$ fs) and a stepwise reaction mechanism [with a fast initial step ($\tau \approx 100$ fs) and a slower final step ($\tau \approx 10$ ps)]. Quantum dynamics simulations on a two-dimensional model reveal that the concerted reaction occurs despite the nonexistence of a concerted reaction path, but they fail to explain the relative slowness of the stepwise mechanism. A qualitative simulation using a three-dimensional model suggests that internal vibrational relaxation (IVR) might be the reason why the second stage of the stepwise mechanism is so slow.

Introduction

The photoinduced excited-state double-proton transfer in 2,2′-bipyridyl-3,3′-diol [henceforth $BP(OH)_2$] has been the target of several experimental[1–5] and theoretical[6–8] studies. This system has an absorption peak at $\lambda = 340$ nm and a broad fluorescence band at $\lambda = 510$ nm. The large Stokes shift (≈ 10000 cm^{-1}) and the relative insensitivity of the absorption and emission maxima towards solvent polarity have been considered strong support for the fluorescent species being the first excited singlet S_1-diketo tautomer with a vanishing dipole moment.

The wealth of knowledge about the excited state double-proton-transfer reaction in $BP(OH)_2$ has increased substantially over the last decade, especially due to the advent of sophisticated experimental techniques, which are able to resolve ultrafast dynamics in the sub-pico- and femtosecond range. The double-proton transfer in $BP(OH)_2$ was thought for some time to be a one-step, concerted process, in which both protons are transferred simultaneously, and which takes place with a characteristic time of ≈ 5 ps. However, sophisticated fluorescence up-conversion and transient absorption experiments in apolar and polar aprotic solvents proved that the process is actually *branched* and consists of a *concerted* reaction channel, where both protons exchange the binding site simultaneously, and a *stepwise* channel, where one proton transfers first and the other transfers upon completion of the first step.[1] The characteristic time for the concerted pathway has been established to be $\tau_c \approx 100$ fs. As for the stepwise pathway, the first process occurs within $\tau_{s1} \approx 100$ fs whereas the second step is much slower ($\tau_{s2} \approx 10$ ps). Figure 1 shows, schematically, the defined reaction mechanisms and establishes the nomenclature of the different species involved for the purposes of this work.

The dynamic properties of this ultrafast complex process have been thoroughly studied. Glasbeek and co-workers discovered that no deuterium isotope effects were present in the stepwise mechanism.[2] Besides, τ_{s1} does not show any dependence either on temperature nor on solvent polarity. On the other hand, τ_{s2} does have a slight dependence on temperature

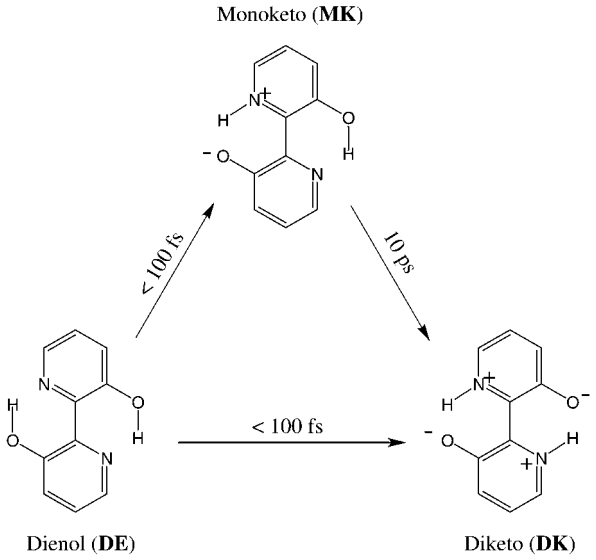

Figure 1. *Possible reaction mechanisms for the double-proton transfer of 2,2′-bipyridyl-3,3′-diol in S_1. The charges shown are formal charges in the context of a Lewis structure and do not necessarily correspond to the actual charge distribution.*

in aprotic polar solvents, which can be quantified in a small activation energy of ≈ 100 cm^{-1}.[2] In a recent paper, anisotropy measurements allowed the monitoring of the disappearance of the dienol tautomer directly, with a characteristic time $\tau \approx$ 350 fs. This process was essentially barrierless.[3]

By a careful selection of the detection wavelength, Glasbeek and co-workers could evaluate the quantities of diketo tautomer (**DK**) obtained through the stepwise and concerted mechanisms. By monitoring the dependence of the ratio of diketo

[a] *Dr. R. Gelabert, Dr. M. Moreno, Prof. J. M. Lluch*
Departament de Química, Universitat Autònoma de Barcelona,
08193 Bellaterra, Barcelona (Spain)
Fax: (+34) 93-581-2920
E-mail: lluch@klingon.uab.es

  DOI: 10.1002/cphc.200400078

tautomer (formed through each mechanism) with the excess energy in the initial state, it was possible to ascertain the presence of an energy barrier in the first stage of the stepwise mechanism. By means of a simple tunneling model, the magnitude of this barrier was estimated to be $\approx 600\ cm^{-1}$. Also, the transit time across the barrier was estimated to be 5 fs.[4] Similar studies performed on $BP(OH)_2$ in sol-gel glasses gave a barrier height of $\approx 300\ cm^{-1}$.[5]

One intriguing feature of this system is: how can it be explained that, although the mechanistic steps are essentially barrierless, the second stage of the stepwise mechanism is still very slow compared to either the first stage of this stepwise mechanism or to the concerted reaction step?

When measuring the amounts of diketo tautomer formed through the intermediate monoketo (**MK**) and directly from the dienol (**DE**), Glasbeek and co-workers discovered that even though the ratios depended on the excitation wavelength, the characteristic reaction times did not.[4] This was interpreted in terms of a relaxation of the intermediate species (**MK**), which occurs before the second step can take place.[4] Besides, if the excitation excess energy is large enough, the initially formed state ought to have no clear preference to evolve directly to **MK** or to **DK**, so that one would expect a statistical value of two for the ratio. However, the ratio leveled off at about 0.7, which clearly showed that the **DE** tautomer in S_1 did not decay completely into **MK** or **DK**, but rather, that some additional relaxation channel must exist to account for the diminution in yield of the **MK** tautomer. This was interpreted as a proof of the competition between the reactive process and internal vibrational relaxation (IVR) processes of the molecule.[4] Besides, in the anisotropy experiments the initial value obtained was smaller than expected (even when the excited state was prepared with excess energy). This loss of anisotropy was also compatible with an intervention of IVR processes in the chromophore. IVR has been described as a very fast process in chromophores with sizes similar to that of $BP(OH)_2$.[9,10]

In this paper, we present a density functional theory (DFT) electronic-structure study of $BP(OH)_2$ in the gas phase followed by nuclear quantum dynamics simulations on a model surface of the system. The goal is to provide insight from the world of theory into the dynamics of this process, with the special aim at explaining the different timescales observed (which have so far been described only experimentally). We would like to mention that the so-called excited-state intramolecular proton transfer (ESIPT) processes have, for some time, been known to be (in many cases) hydrogen-transfer processes. Nevertheless, it is usual in scientific literature to refer to ESIPT processes as proton-transfer processes. In the present work, we have opted for the "proton transfer" term, in the understanding that the purpose of this paper is not to discuss the chemical nature of the entity being transferred (a goal towards which no steps have been taken herein) but rather the elucidation of the intricacies involved in the reaction mechanism.

Results and Discussion

To initiate the study, the stationary points in the ground electronic state (S_0) potential energy surface (PES) have been located (by full minimization) and characterized. Also, single-point, unoptimized TDDFT calculations have been carried out in order to estimate the energy landscape in the S_1 excited state. TDDFT was used to study this same system recently and was proven to perform well.[8] Results are displayed in Figure 2.

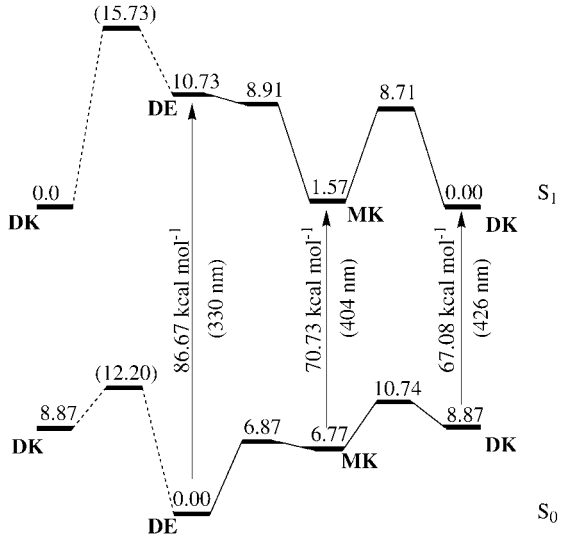

Figure 2. *Energies [kcal mol^{-1}] of the stationary points in S_0 relevant to the double-proton transfer (bottom). The upper half of the figure shows the energies of the previous structures in S_1 (unoptimized). The energy of the vertical transitions and their wavelengths are also shown. Values in parentheses correspond to second-order saddle points.*

The most stable structure in S_0 is the dienol tautomer. Three other minima exist. Two of them are identical and correspond to a structure in which only one of the protons has actually been transferred. This is the intermediate in the stepwise mechanism (**MK**), and lies $+6.77\ kcal\,mol^{-1}$ above the dienol structure. The other minimum is the diketo (**DK**), or final product of the double-proton transfer, at $+8.87\ kcal\,mol^{-1}$. The localization of higher-order stationary points produced two pairs of transition-state structures. These correspond to the two transition-state structures for the transformations **DE**→**MK** ($+6.87\ kcal\,mol^{-1}$) and **MK**→**DK** ($+10.74\ kcal\,mol^{-1}$). Finally, there is a second-order saddle point in the configurational region, in which a tentative transition state for the concerted mechanism should be, with an energy of $+12.20\ kcal\,mol^{-1}$ with respect to the dienol structure.

It is possible to guess how the S_1 surface looks by computing the vertical excitation energy on all the stationary points found on the S_0 surface. These results are also depicted in Figure 2. Although qualitative, this is a first hint as to what the energy landscape in S_1 might look like. Based on this, the most stable structure in S_1 would be the diketo tautomer, almost degenerate to the monoketo tautomer. There could be a small energy barrier ($\approx 1\ kcal\,mol^{-1}$) for the transfer from S_1-**DE** to S_1-

MK. The barrier separating S_1-**MK** and S_1-**DK** could be substantial ($\approx$7–9 kcal mol^{-1}).

The examination of the electronic wave function of the studied S_1 points reveals that the nature of the excitation involved is $\pi^*\leftarrow\pi$. It is interesting to note that the estimated wavelengths for excitation and fluorescence do not agree completely with the experimental values. In fact, the ordering reported from the experiments is $\lambda_{DE}<\lambda_{DK}<\lambda_{MK}$ whereas the ordering suggested by our calculations is $\lambda_{DE}<\lambda_{MK}<\lambda_{DK}$. However, it is important to take into account that, to satisfactorily compare our calculations with the available experimental data, it is necessary to include vibrational contributions, which are missing in this simplified preliminary study. However, even without these vibrational contributions, there is a good agreement between our theoretical calculations ($\lambda=330$ nm) and the experiment ($\lambda=340$ nm) for the S_1-**DE**$\leftarrow S_0$-**DE** transition.

From the pure electronic structure calculations just discussed, it is possible to assume that, for the S_0 and probably also for the S_1 states, the double-proton transfer occurs through a stepwise mechanism. This mechanism would be based, in the ground state, on the nonexistence of a proper transition state for the concerted process (instead, a second-order stationary point has been found), and in the excited state, on the similarity of topologies so far found. However, this process has been described as "ultrafast" and is initiated after the photoabsorption of the dienol tautomer has occurred. The excess energy of the dienol tautomer in the S_1 state, immediately after photoabsorption, makes it unlikely that potential energy barriers alone can be sufficient to quantify the reaction rate or decide for a mechanism. Dynamical calculations are needed.

To correctly simulate the process, we need a representative portion of the S_1 electronic state. From the experimental evidence, it seems clear that one should consider two different possibilities for the reaction at hand (concerted and stepwise), and that the proposed potential energy surface should be flexible enough to contain both dynamical paths. The surface must be then, at least, 2D: one degree of freedom should represent the concerted, one-step mechanism, and the other should represent the stepwise mechanism. Since nuclear dynamics calculations will be carried out on this potential energy surface, it is necessary to know, in an explicit way, the mass associated to each degree of freedom involved.

It has been suggested in the literature that each possible reaction pathway can be activated by different promoting modes in $BP(OH)_2$.[2,4] To be precise, it seems reasonable that the concerted double-proton transfer is to be assisted by the normal mode, which describes the stretching of the central C–C bond between the pyridyl rings, while the stepwise mechanism is to be assisted by the bending mode of one pyridyl ring with respect to the other. This means that, to include the effect of these modes explicitly, one should actually build a four-dimensional hypersurface. Since we are interested in performing an approximate treatment of $BP(OH)_2$, we will not consider the effect of these two specific modes in our simulations.

It is tempting to design this reduced potential energy surface by fixing the geometry of the two proton transfers at different values and allowing the system to relax. While this would guarantee that the built potential energy surface has the lowest energies possible, it is at least debatable that, in an ultrafast process, the protons would move adiabatically (i.e., this would mean that the rest of the nuclei are moving much faster than them). Besides, this kind of treatment does not make a clear assignment of masses to every degree of freedom of the surface (the identity of the atoms that move and the extent of the motion is changing all over the surface).

In this study we have chosen to define the potential energy surface as a plane in the full 3*N* space [Equation (1)]:

$$\vec{Q}(u,v) = \vec{Q}_0 + u\hat{u} + v\hat{v} \tag{1}$$

where $\vec{Q}_0$ is a fixed point in the plane, and $\hat{u}$ and $\hat{v}$ are two convenient unit vectors. $\vec{Q}(u,v)$ is, obviously, a two-dimensional surface. In our case, an appropriate choice for $\vec{Q}_0$ would be a point close to all the relevant stationary points in the reaction. Convenient choices for $\hat{u}$ and $\hat{v}$ would be vectors, which describe the motion of the protons in both the concerted and the stepwise mechanisms (or a combination of both). The choice of the three parameters in Equation (1) is described below.

Let $\vec{q}_{DE}$ be the 3*N*-dimensional mass-weighted Cartesian vector, which describes the geometry of the dienol tautomer in the S_0 state. Let $\vec{q}_{DK}$, $\vec{q}_{MK1}$, and $\vec{q}_{MK2}$ be the corresponding vectors for the diketo tautomer and the two monoketo tautomers obtained when either of the protons has been already transferred. These four points do not necessarily define a plane. We define now the following vectors [Equations (2)]:

$$\vec{u} = \vec{q}_{DK} - \vec{q}_{DE} \tag{2a}$$

$$\vec{v} = \vec{q}_{MK1} - \vec{q}_{MK2} \tag{2b}$$

Considering the starting and ending points of $\vec{u}$, one may conclude that this vector describes the synchronous motion of each proton from the donor to the acceptor, and is a good candidate for representing the concerted reaction pathway. Similar considerations reveal that $\vec{v}$ describes the synchronous motion of two protons from one pyridyl ring to the other. Both vectors would describe the regions of the potential energy surface that are interesting for solving our problem, provided that an adequate point $\vec{Q}_0$ (which should be more or less equidistant to points $\vec{q}_{DE}$, $\vec{q}_{MK1}$, $\vec{q}_{MK2}$, and $\vec{q}_{DK}$) is defined. A convenient choice for $\vec{Q}_0$ would then be Equation (3):

$$\vec{Q}_0 = \frac{1}{4}(\vec{q}_{DK} + \vec{q}_{MK1} + \vec{q}_{MK2} + \vec{q}_{DE}) \tag{3}$$

We think that the 2D surface defined by Equations (1), (2), and (3) is a good low-dimensional model because it is close to all stationary points in the complete 3*N* configurational space. Computing $\hat{u}$ and $\hat{v}$ in mass-weighted Cartesian coordinates and building the potential energy surface accordingly means that the u and v degrees of freedom represent a collective motion with a clear, unique mass assignment. Hence, dynamics calculations can be carried out without any ambiguity. Finally, we remark that points $\vec{q}_{DE}$, $\vec{q}_{DK}$, $\vec{q}_{MK1}$, and $\vec{q}_{MK2}$ have previ-

ously been translated, to eliminate shifting of the center of mass, and oriented (rotated), to achieve the maximum superposition of their structures. The actual 2D potential energy hypersurface is then formally defined as [Equation (4)]:

$$V_i^{2D}(u,v) = V_i[\vec{Q}(u,v)] \quad (4)$$

where $V_i[\vec{Q}(u,v)]$ represents the electronic plus internuclear repulsion energies of a structure defined by $\vec{Q}(u,v)$ in the ith electronic state.

Table 1 displays the mass-weighted distances between the different points involved in the determination of this potential energy surface. As mentioned above, points $\vec{q}_{DE}$, $\vec{q}_{MK1}$, $\vec{q}_{MK2}$, and $\vec{q}_{DK}$ do not necessarily define a plane. Nonetheless, the extent to which the approximate potential energy surface is good enough to study the dynamics of the real system depends on how close it is to the four points chosen. One way to estimate this closeness is as follows: one can imagine two planes, the first defined by points $\vec{q}_{DE}$, $\vec{q}_{MK1}$, and $\vec{q}_{MK2}$, and the second defined by points $\vec{q}_{MK1}$, $\vec{q}_{MK2}$, and $\vec{q}_{DK}$. Except when both planes are parallel, they intersect in the line defined by points $\vec{q}_{MK1}$ and $\vec{q}_{MK2}$, which is actually the "hinge" between both. The angle defined by the two planes can be used as a measure of the suitability of $\vec{Q}(u,v)$ as a reduced representation of the full hypersurface (this representation being optimal when the angle is 180 degrees). The actual value for our fit is 145.0 degrees.

Table 1. *Mass-weighted distances between minima in S_0.*[a]

Path	Length [amu$^{1/2}$ Å]
DE→**MK1**	0.8538
DE→**MK2**	0.8538
DE→**DK**	1.0989
MK1→**MK2**	1.2942
MK1→**DK**	0.8793
MK2→**DK**	0.8793

[a] **MK1** and **MK2** refer to the two equivalent minima in which only one proton has actually been transferred.

Based on this model, meshes of 23 points for the $\hat{u}$ direction and 33 points for the $\hat{v}$ direction were determined; these represent different configurations relevant to the double-proton transfer process in $BP(OH)_2$. A single-point TDDFT calculation was performed at each of these points and the resulting mesh fitted into a cubic splines functional form.[11] Figure 3 shows the reduced-dimensionality potential energy surfaces built using this procedure for the S_0 and S_1 electronic states respectively; these potential energy surfaces will be the basis of the dynamics simulations described below. As a measure of the accuracy of the fit, the relative stabilities of the **DE**, **MK**, and **DK** minima in S_0 obtained from the fit and from the complete optimizations were compared; these were found to agree within a range of 0.05 kcal mol^{-1}. The first-order stationary points differ by 2–4 kcal mol^{-1}, and the second-order saddle point differs by more than approximately 5 kcal mol^{-1}. However, it is unlikely that a second-order saddle point will have a dynamical relevance in the process.

It is worth examining the S_1 reduced surface with greater detail. For this an in-depth exploration of the potential energy surface for this state is required. The stationary points have been relocalized in this reduced potential energy surface. The most stable structure is the **DK**, in agreement with the experimental data. The **MK** structure is at $+1.47$ kcal mol^{-1}, whereas the **DE** structure is at $+10.44$ kcal mol^{-1}. In the reduced surface, the transition state that connects the **DE** and **MK** structures is 1.30 kcal mol^{-1} over the S_1-**DE** minimum or 1.01 kcal mol^{-1} above the Franck–Condon region. These values agree well with the barrier estimated by Marks et al.[4] of 600 cm^{-1} or 1.7 kcal mol^{-1}. We consider this to be a proof of the correctness of the potential energy surface we have built for S_1.

As for the expected dynamical behavior, the topology of S_1 seems to indicate that no concerted mechanism can take place. The concerted mechanism transition-state structure is actually a maximum in the reduced-potential energy surface and also a second-order saddle point in the full dimensionality surface.

We are in a position to carry out nuclear dynamics simulations. Because the surface is just a 2D surface, it is possible to use quantum dynamics directly. The methodology used has been a standard split-time propagation-scheme procedure,[12,13] in which fast Fourier transform (FFT) is used to transform the wave packet from position to momentum space and vice versa. To simulate the experimental setup, the initial state of the simulation is prepared as the harmonic approximation to the vibrational ground state on S_0. This state is nonstationary in S_1 and evolves with time.

To analyze the time scales of the process, the probability density ($|\psi(t)|^2$) is integrated at each time step over certain regions of the surface around the **DE**, **MK**, and **DK** minima. In this way the time scale of the **DE**→**MK** reaction can be monitored by computing the density on the **MK** and **DE** minima. Figure 4 depicts the integral of density in areas surrounding the minima. The regions are defined as circular areas, centered at the minimum and with a radius that is large enough to en-

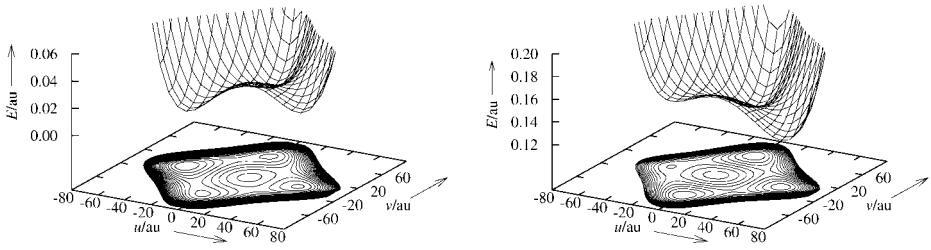

Figure 3. *Combined surface and contour plot of the potential energy surfaces of S_0 (left) and S_1 (right). All magnitudes are in atomic units. In both graphs, the* **DE** *minimum is on the left end ($v = 0$, $u < 0$) and the* **DK** *minimum on the right end ($v = 0$, $u > 0$). For clarity reasons, only half of the surface is shown in the 3D perspective ($v > 0$). For the definition of $\vec{u}$ and $\vec{v}$ see Equation (2).*

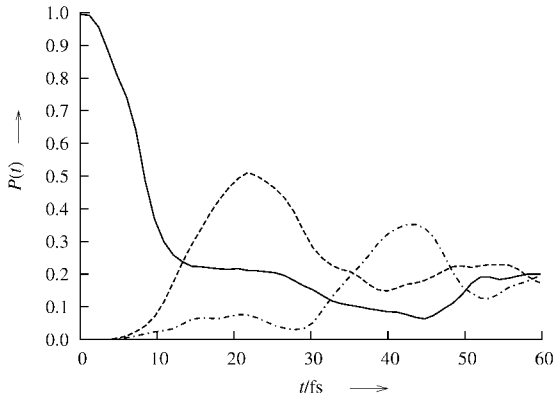

Figure 4. *Integral of density in the areas close to the* **DE** *minimum (——), **MK** minima (-----), and* **DK** *minimum (–•–•) in the two-dimensional model.*

compass the concave area in the surrounding. Hence, the sum of the dienol, diketo, and monoketo densities does not necessarily add up to one.

Figure 4 reveals some interesting points. It can be seen that, initially, the dienol species disappears quickly (within 20 fs). This process occurs simultaneously with an increase in the amounts of monoketo and, to a lower extent, diketo species. Actually, the monoketo—the most affordable species from an energetic point of view—appears first, with a density maximum around 20 fs after the beginning of the reaction. However, the diketo species goes through a maximum at the same time, though this maximum is less prominent. This means that the reaction does not proceed completely from dienol to monoketo (that is, through a stepwise mechanism) because a significant density appears as diketo species (via a concerted pathway). These results and the timescales found are in good agreement with the experimental data available.

The second stage in the stepwise mechanism can also be observed in Figure 4 as a second, more prominent maximum of density of the diketo species (after 40 fs). This maximum coincides with a minimum of the monoketo species, which is an unambiguous indication that this maximum has its origin in the **MK**→**DK** reaction step. This is also a very fast process (despite the fact that the energy barrier is in excess of 8 kcal mol^{-1}, measured from the bottom of the **MK** minimum). Since the system, immediately after the photoexcitation, has enough energy to cross this barrier, the reaction occurs as if there were no barrier at all. Finally, at longer times, Figure 4 reveals that the amount of dienol species increases again. This has to be interpreted as being due to the bouncing back of the time-evolved wave packet, which can go nowhere else in this 2D model surface. Hence, this "bouncing back" has no physical significance in the real system, and the simulation is stopped. In the real system, the existence of several extra degrees of freedom coupled to the ones considered here would allow part of the energy of the initial wave packet to excite these degrees of freedom. As such, this fact would likely "trap" the wave packet before it can cross the barrier that separates the monoketo and diketo species.

An inclusion of the complete set of extra degrees of freedom is unaffordable, and modeling is needed. To simulate the existence of these degrees of freedom and see whether it is possible to observe any changes in the dynamics of the system as far as the **MK**→**DK** reaction is concerned, we have modified the model potential by adding a single extra degree of freedom [Equation (5)]:

$$V_{S_1}^{3D}(u,\nu,Q) = V_{S_1}^{2D}(u,\nu) + \frac{1}{2}\omega^2\left[Q - \frac{c}{\omega^2}|\nu|\right]^2 \qquad (5)$$

where $V_{S_1}^{2D}(u,\nu)$ is the 2D potential energy surface used in the previous simulation. The third degree of freedom, Q, is represented as a simple shifted harmonic oscillator of frequency ω and coupling constant c. Naturally, the purpose is not to obtain a quantitative agreement between the simulations based on this model and the experiments, but rather, to explore what the effect of this extra degree of freedom is on the rate of the second stage of the stepwise mechanism.

We have no information that allows us to select values for c and ω. Instead, we have carried out a systematic study of the influence of these parameters on the population-evolution diagrams, taking into account that the choice of these parameters should not change the nature of the process significantly.

The results of the simulations of the 3D model with a medium coupling constant ($c = 4.7\times10^{-6}$ au) and several frequencies for the coupled harmonic mode ω, which describes the coupling to a mode with frequencies between 300 and 1000 cm^{-1}, are depicted in Figures 5 (monoketo) and 6 (diketo). In both Figures, the results obtained previously for the 2D model are included for comparison purposes.

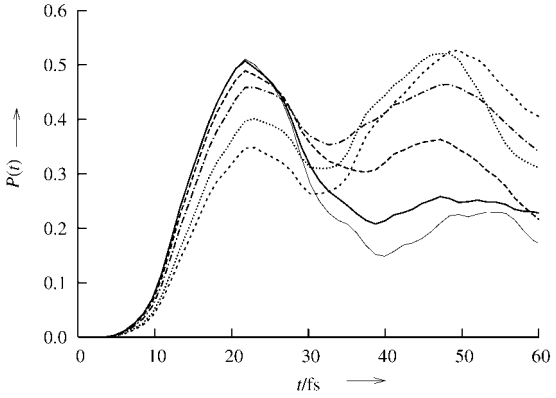

Figure 5. *Integral of density around the **MK** minima in the 3D model for the following frequencies of the coupled oscillator: 1000 cm^{-1} (thick solid), 690 cm^{-1} (long dashed), 500 cm^{-1} (dot–dash), 380 cm^{-1} (thin dot), and 340 cm^{-1} (thick dot). For comparison purposes, the results obtained with the 2D model are also included (thin solid).*

It is possible to see that, for this coupling constant, the results obtained with the 2D model agree with those obtained with the 3D model only when the coupled frequency is high enough. The inclusion of a slower vibrational mode causes a decrease in the amount of monoketo species formed in the

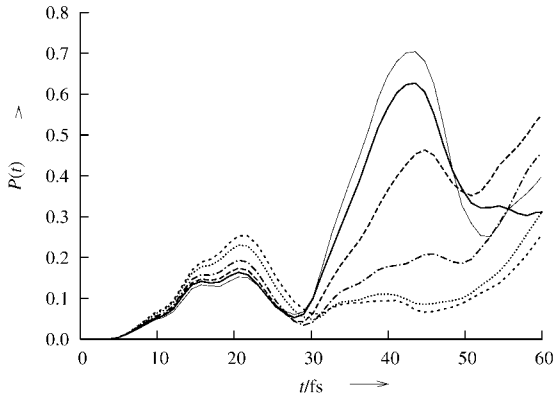

Figure 6. *Integral of density around the* **DK** *minimum in the 3D model for the following frequencies of the coupled oscillator: 1000 cm^{-1} (thick solid), 690 cm^{-1} (long dashed), 500 cm^{-1} (dot–dash), 380 cm^{-1} (thin dot), and 340 cm^{-1} (thick dot). For comparison purposes, the results obtained with the 2D model are also included (thin solid).*

first stage of the stepwise mechanism, without noticeably changing the time it takes to reach the maximum of density of the monoketo species (which is $t \approx 20$ fs). Exactly the opposite happens to the diketo species formed through the concerted mechanism. It seems then that the presence of a slow vibrational mode favors the concerted reaction **DE**→**DK** over the first step of the stepwise mechanism, **DE**→**MK**. However, the most striking effect can be observed on the second maximum in the diketo population (Figure 6), which corresponds to the diketo tautomer formed through the stepwise mechanism. The height of this maximum clearly decreases when the frequency is decreased and, actually, it even disappears for the slowest modes. In agreement with this, the minimum of the population of monoketo species, which appeared in the 2D simulation at $t \approx 40$ fs, progressively disappears when the frequency of the oscillator decreases. We think that this result is in good agreement with the experimentally reported deviation from the statistical value of two for the ratio of diketo tautomer formed through the stepwise and concerted mechanisms.

The model we have used is simple and, hence, only qualitative conclusions can be drawn from it. The fact that coupling the system to a harmonic oscillator reduces the effectivity of the second stage of the stepwise mechanism is, however, significant. From Figures 5 and 6, it appears that the system becomes increasingly trapped in the **MK** region when a slow oscillator is coupled to it. In this way, the efficiency of the second stage of the stepwise mechanism is reduced. In our opinion, it is possible to extrapolate these results to the full system, in which many more coupled degrees of freedom exist. In this case, the completion of the second stage of the stepwise mechanism could take place in a longer time scale of about 10 ps.

These results, even though qualitative, seem to confirm that some internal vibrational relaxation (IVR) mechanism may be competing with the stepwise mechanism, making the second step of the latter considerably slower. This effect is purely dynamical in nature, and is beyond the descriptive capabilities of statistical theories such as transition-state theory (TST).

Conclusions

In this paper we have presented a combined electronic structure DFT and nuclear quantum dynamics study of the double-proton transfer reaction in 2,2′-bipyridyl-3,3′-diol in the first excited singlet state, which, according to experimental data, can occur via a branched process, which consists of a concerted mechanism (faster than 100 fs) and a stepwise mechanism (with a first stage that is faster than 100 fs and a second stage that is much slower, in the 10 ps range). A model 2D surface has been built for this system in the S_0 and S_1 electronic states to describe both reaction mechanisms. The lack of a transition state in the S_1 electronic state, which describes the concerted proton-transfer mechanism, seems to indicate that only the stepwise mechanism is to be expected. Nuclear dynamics calculations on S_1, which simulate the experimental setup on this 2D surface correctly, account for the rate of the first stage of the stepwise mechanism. Also, it is seen that, despite the lack of a proper transition-state structure, some product is formed directly through a concerted mechanism. The rate of this last process is also correctly accounted for. The simulation, however, reveals that the second stage of the stepwise mechanism is as fast as the first one.

To explain the experimental evidence, the model surface used was enlarged to include a shifted coupled harmonic oscillator for simulating, qualitatively, the internal vibrational relaxation (IVR). With this enlarged model, the amount of product formed through the stepwise mechanism was observed to decrease with the frequency of the coupled mode, because the system gets trapped in the monoketo minimum. These results could be extrapolated to the full system, with many more coupled degrees of freedom, where we expect that the completion of the second stage of the stepwise mechanism would take place in a longer time scale, similar to that reported experimentally (10 ps). This indicates that IVR may be the reason for the large difference in speed observed between both stages of the stepwise mechanism.

Computational Methods

Two different sets of calculations were necessary to study the dynamics of the ultrafast double-proton transfer in $BP(OH)_2$. Firstly, electronic-structure calculations were used to study the topology of the ground and first singlet excited states, and to build a reduced-dimensionality representation of the potential energy hypersurface of the double-proton transfer. Secondly, dynamical calculations were carried out on the S_1 potential energy surface to quantify the timescales of the process. Details of both sets of calculations follow.

All electronic-structure calculations were carried out with the Gaussian 98 program.[14] For the ground state calculations, the DFT methodology was chosen,[15,16] and more precisely, the three parameter hybrid functional of Becke with the correlation functional of Lee, Yang, and Parr (B3LYP).[17–19] The basis set chosen was 6–31G(d),[20] which made the computation of a sizeable portion of the PES affordable. The calculations for the S_1 electronic state were computed with the time-dependent formalism,[21–23] using the same base functional as in the ground state. Stationary points in the ground state were located using the Schlegel optimization al-

gorithm within a redundant coordinate framework[14,24] and, when necessary, characterized through diagonalization of the Hessian matrix. No optimizations were performed for the S_1 electronic state calculation.

The method chosen for determining the timescale of the reactive processes in the S_1 excited state was the wave packet propagation. To simulate the experimental setup, one prepares the initial state of the simulation by setting up an appropriate wave function (e.g. an approximation to the S_0 ground vibrational state) and placing it into the Frank–Condon region in the S_1 excited state. This wave function does not represent a stationary state of S_1 and, in order to establish the time evolution of this state, the time-dependent Schrödinger equation [Eq. (6)] needs to be solved:

$$i\hbar\frac{\mathrm{d}}{\mathrm{d}t}|\psi\rangle = \hat{\mathscr{H}}|\psi\rangle \tag{6}$$

or, equivalently [Eq. (7)], given that the Hamiltonian is time-independent:

$$|\psi\rangle = e^{-i\hat{\mathscr{H}}t/\hbar}|\psi_0\rangle \tag{7}$$

where [Eq. (8)]:

$$\hat{\mathscr{H}} = \hat{T} + \hat{V}_{S_1}(\vec{q}) \tag{8}$$

Here, $\vec{q}$ is the set of coordinates upon which the potential energy surface is defined. To solve Equation (7), a standard split-time propagator scheme was used.[12,13] The propagation proceeds by applying a split-operator propagator over a short time interval Δt [Equation (9)]:

$$e^{-i\hat{\mathscr{H}}t/\hbar} \approx e^{-i\hat{V}\Delta t/2\hbar}\, e^{-i\hat{T}\Delta t/\hbar}\, e^{-i\hat{V}\Delta t/2\hbar} \tag{9}$$

That is, during each time step the potential energy propagator is initially applied for half a time step; this is then followed by the kinetic energy propagator, which is applied for a full time step, and finally, the potential energy propagator is applied for another half a time step. The split-operator scheme just described is applied to minimize propagation errors, because $\hat{T}$ and $\hat{V}$ do not commute.

Fast Fourier transform (FFT) was applied to transform the wave function from position to momentum representation (and vice versa) in between any two propagators in Equation (9). The size of the FFT grid was of 2^6 points per dimension, and the time step in the propagation was $\Delta t = 0.1$ atu (1 atu $= 2.419\times10^{-17}$ s). In all simulations the norm of the wave function was preserved to three significant figures. We note that, due to the specific characteristics of the potential energy surfaces used, there was no need to use absorbing potentials at the edges of the FFT grid.

Acknowledgements

R.G. gratefully acknowledges the support of the Spanish "Ministerio de Ciencia y Tecnología" by means of a "Ramón y Cajal" research contract. The authors are grateful for financial support from the Spanish "Ministerio de Ciencia y Tecnología" and the "Fondo Europeo de Desarrollo Regional" through project BQU2002–00301.

Keywords: excited states · femtochemistry · proton transfer · quantum dynamics · reaction mechanisms

[1] H. Zhang, P. van der Meulen, M. Glasbeek, *Chem. Phys. Lett.* **1996**, *253*, 97–102.
[2] D. Marks, H. Zhang, M. Glasbeek, P. Borowicz, A. Grabowska, *Chem. Phys. Lett.* **1997**, *275*, 370–376.
[3] P. Toele, H. Zhang, M. Glasbeek, *J. Phys. Chem. A* **2002**, *106*, 3651–3658.
[4] D. Marks, P. Prosposito, H. Zhang, M. Glasbeek, *Chem. Phys. Lett.* **1998**, *289*, 535–540.
[5] P. Prosposito, D. Marks, H. Zhang, M. Glasbeek, *J. Phys. Chem. A* **1998**, *102*, 8894–8902.
[6] V. Barone, C. Adamo, *Chem. Phys. Lett.* **1995**, *241*, 1–6.
[7] A. L. Sobolewski, L. Adamowicz, *Chem. Phys. Lett.* **1996**, *252*, 33–41.
[8] V. Barone, A. Palma, N. Sanna, *Chem. Phys. Lett.* **2003**, *381*, 451–457.
[9] G. De Belder, G. Schweitzer, S. Jordens, M. Lor, S. Mitra, J. Hofkens, S. De Feyter, M. Van der Auweraer, A. Hermann, T. Weil, K. Müllen, F. C. De Schryver, *ChemPhysChem* **2001**, *2*, 49–55.
[10] P. T. Chou, Y. C. Chen, W. S. Yu, Y. H. Chou, C. Y. Wei, Y. M. Cheng, *J. Phys. Chem. A* **2001**, *105*, 1731–1740.
[11] W. H. Press, B. P. Flannery, S. A. Teulkolsky, W. T. Vetterling, *Numerical Recipes in FORTRAN*, 2nd Edition, Cambridge University Press, Cambridge, **1992**.
[12] M. D. Feit, J. A. Fleck, A. Steiger, *J. Comput. Phys.* **1982**, *47*, 412–433.
[13] R. Kosloff, *J. Phys. Chem.* **1988**, *92*, 2087–2100.
[14] Gaussian98 (Revision A.11), M. J. Frisch, G. W. Trucks, H. B. Schlegel, G. E. Scuseria, M. A. Robb, J. R. Cheeseman, V. G. Zakrzewski, J. A. Montgomery Jr., R. E. Stratmann, J. C. Burant, S. Dapprich, J. M. Millam, A. D. Daniels, K. N. Kudin, M. C. Strain, O. Farkas, J. Tomasi, V. Barone, M. Cossi, R. Cammi, B. Mennucci, C. Pomelli, C. Adamo, S. Clifford, J. Ochterski, G. A. Petersson, P. Y. Ayala, Q. Cui, K. Morokuma, D. K. Malick, A. D. Rabuck, K. Raghavachari, J. B. Foresman, J. Cioslowski, J. V. Ortiz, A. G. Baboul, B. B. Stefanov, G. Liu, A. Liashenko, P. Piskorz, I. Komaromi, R. Gomperts, R. L. Martin, D. J. Fox, T. Keith, M. A. Al-Laham, C. Y. Peng, A. Nanayakkara, M. Challacombe, P. M. W. Gill, B. Johnson, W. Chen, M. W. Wong, J. L. Andres, C. Gonzalez, M. Head-Gordon, E. S. Replogle, J. A. Pople, Gaussian, Inc., Pittsburgh, PA, **1998**.
[15] R. G. Parr, W. Yang, *Density Functional Theory of Atoms and Molecules*, Oxford University Press, Oxford, **1989**.
[16] T. Ziegler, *Chem. Rev.* **1991**, *91*, 651–667.
[17] C. T. Lee, W. T. Yang, R. G. Parr, *Phys. Rev. B* **1988**, *37*, 785–789.
[18] A. D. Becke, *J. Chem. Phys* **1993**, *98*, 5648–5652.
[19] P. J. Stephens, F. J. Devlin, C. F. Chabalowski, M. J. Frisch, *J. Phys. Chem.* **1994**, *98*, 11 623–11 627.
[20] M. M. Francl, W. J. Pietro, W. J. Hehre, J. S. Binkley, M. S. Gordon, D. J. DeFrees, J. A. Pople, *J. Chem. Phys.* **1982**, *77*, 3654–3665.
[21] R. Bauernschmitt, R. Ahlrichs, *Chem. Phys. Lett.* **1996**, *256*, 454–464.
[22] M. E. Casida, C. Jamorski, K. C. Casida, D. R. Salahub, *J. Chem. Phys.* **1998**, *108*, 4439–4449.
[23] R. E. Stratmann, G. E. Scuseria, M. J. Frisch, *J. Phys. Chem.* **1998**, *109*, 8218–8224.
[24] C. Y. Peng, P. Y. Ayala, H. B. Schlegel, M. J. Frisch, *J. Comput. Chem.* **1996**, *17*, 49–56.

Received: February 24, 2004

